ELSEVIER

Marine Geology 192 (2002) 105–121

MARINE GEOLOGY
INTERNATIONAL JOURNAL OF MARINE GEOLOGY, GEOCHEMISTRY AND GEOPHYSICS

www.elsevier.com/locate/margeo

Laboratory experiments and numerical simulation of sediment-wave formation by turbidity currents

Yu'suke Kubo [a,*], Takeshi Nakajima [b]

[a] *Department of Geology and Mineralogy, Graduate School of Science, Kyoto University, Kyoto 606-8502, Japan*
[b] *Fuel Resource Geology Research Group, Institute for Geo-Resources and Environment, Geological Survey of Japan/AIST, Site C-7, 1-1-1 Higashi, Tsukuba, Ibaraki 305-8567, Japan*

Received 9 November 2000; received in revised form 8 May 2001; accepted 2 August 2002

Abstract

This paper presents the results of laboratory experiments and numerical simulations carried out in order to understand the mechanism of sediment-wave formation by turbidity currents. Experimental turbidity currents were generated in a 10-m-long laboratory flume, so as to investigate the topographic effects of slope and ridges on turbidite deposition. The results indicate that preferential deposition occurs on the upstream side of the ridges. This preferential deposition is considered to result in possible upstream migration of the topography, a common feature of deep-sea sediment waves, provided that such deposition were repeated. The preferential deposition occurred under a subcritical turbidity current, implying that antidune flow conditions ($0.844 < Fr < 1.77$) are not necessarily required for upstream migration of the bedforms. A numerical simulation using layer-averaged Navier–Stokes equations is successfully applied to the laboratory experiments, and then to deep-sea turbidity currents. The numerical model predicts the formation of a wavy structure in a sequence of thousands of turbidites, with wave dimensions and internal architecture similar to deep-sea sediment waves. The wavy structure is interpreted to form as a succession of mounds, each of which grows individually rather than simultaneously as a sinusoidal wave. Each mound is developed by preferential deposition downstream of a slope break, which in turn generates a new slope break on its downstream side flank. Upstream migration of the waveform results from differential deposition between the upstream and downstream sides of the mounds. These results indicate that neither antidunes nor lee-waves are necessary for the formation and upstream migration of the wavy structure. Wave formation as a series of individual mounds can be considered as an origin for relatively small sediment-wave fields, because no more than 4–5 crests are formed in the model predictions. It is suggested that more extensive sediment-wave fields can be developed by turbidite deposition on an initially undulating bottom, which results in upstream migration by differential deposition, and downstream extension of the wave field by mound formation progressively further downstream.

Keywords: sediment wave; turbidity current; laboratory experiment; numerical simulation

1. Introduction

Deep-sea sediment waves are regular bed undulations on a relatively large scale, with typical

* Corresponding author. Present address: INSTAAR, University of Colorado, 1560 30th Street, Campus Box 450, Boulder, CO 80309-0450, USA. Fax: +1-303-492-6388.
E-mail address: yusuke.kubo@colorado.edu (Y. Kubo).

0025-3227/02/$ – see front matter
PII: S0025-3227(02)00551-0

wave heights of tens of metres and wavelengths of a few kilometres. The crest lines are continuous for several kilometres and are either perpendicular or parallel to the current direction, depending on the mode of formation. These waves have been interpreted as depositional bedforms produced by submarine flows due to their regular shape, and the continuous internal layering indicates upstream migration of the waveform through time (Nakajima, 1997; Nakajima and Satoh, 2001; Normark et al., 1980; Piper and Savoye, 1993; Wynn et al., 2000a,b).

Two types of submarine flows, alongslope bottom currents and downslope turbidity currents, are considered to be responsible for the development of sediment waves. The nature of the flow is, however, considerably different between continuous, almost steady bottom currents and episodic, short-lived turbidity currents. Different mechanisms have therefore been considered for turbidity-current generated (TC) and bottom-current generated (BC) sediment waves, even though these waves apparently display quite similar features. The most widely accepted model for BC sediment-wave formation is the 'lee-wave model' proposed by Flood (1988). Lee-waves are generated in a stratified flow crossing over a topographic high (Queney, 1948; Miles, 1968), and lead to preferential deposition or less erosion on the upstream flank of the wave. Flood (1988) quantified this process to determine the effects of mean flow velocity on migration patterns of sediment waves.

For generation of TC sediment waves, on the other hand, application of the lee-wave model is considered to be inappropriate (Piper and Savoye, 1993; Wynn et al., 2000b; Nakajima and Satoh, 2001). Lee-waves can form in a stratified flow only when the stratification Froude number, determined as U/NH where U is the velocity, N is the buoyancy frequency, and H is the flow thickness, is less than $1/\pi$ (Yih, 1969; Allen, 1982b). Wynn et al. (2000b) showed, however, that this criterion was unlikely to agree with the flow conditions for turbidity currents in the Selvage sediment-wave field. Based on data from seven TC sediment-wave fields, Wynn et al. (2000b) suggested that lee-waves are not responsible for creating TC sediment waves.

Alternatively, TC sediment waves have been interpreted to form as giant antidunes, based on their observed pattern of upstream migration (e.g. Normark et al., 1980; Wynn et al., 2000a,b). The antidune model is supported by Hand's (1974) experiments of antidune-type bedforms produced by a supercritical density current in a laboratory flume. He suggested that antidunes produced by deep-sea turbidity currents were likely to have wavelengths of tens to hundreds of metres, and inferred the applicability of his experimental results to deep-sea sediment waves. Several attempts have been made to estimate palaeocurrent conditions from features of deep-sea sediment waves by applying the criteria for laboratory-scale antidunes (Normark et al., 1980; Piper and Savoye, 1993; Wynn et al., 2000a,b).

However, the antidune model should be applied carefully to TC sediment waves, because the wave theory of bedforms assumes steady flow conditions (Allen, 1982a; Nakajima and Satoh, 2001). Sediment waves are made up of a number of turbidite beds and are therefore produced by multiple flow events. Each flow is considerably short-lived compared to the time scale of sediment-wave formation. Even within each event, a turbidity current tends to be unsteady, as shown by the vertical variation of sedimentary structures in turbidites (Bouma, 1962). Although an antidune origin should not be ruled out, the exact mechanism of sediment-wave formation by turbidity currents is still poorly understood.

This paper describes laboratory experiments and numerical calculations to model the formation of deep-sea sediment waves by turbidity currents. The purposes of the present study are to discuss the applicability of previous models of sediment-wave formation, and to propose an alternative model based on the results of the laboratory experiments and the numerical simulations.

2. Laboratory experiments

The laboratory experiments were carried out in a flume of 10 m length, with a rectangular cross-section 0.2 m wide and 0.5 m deep. For the tur-

bidity current experiments, a gate box of 0.5 m length was inserted at the upstream end of the flume. A surge-type turbidity current was generated by the instantaneous release of a suspension cloud from the gate. The lock exchange is a common method to produce turbidity currents in laboratory experiments (e.g. Middleton and Neal, 1989; Bonnecaze et al., 1993; Gladstone et al., 1998). The suspension cloud contained 2% of fine sand by volume fraction, with median settling velocities of 0.009 m/s (corresponding to 3.2 ϕ in grain size) or 0.006 m/s (3.5 ϕ). To simulate turbidite deposition across sediment waves, a chain of ridges was added to an otherwise horizontal bed (Fig. 1). Each ridge had a height of 0.012–0.036 m and a longitudinal length of 1–2 m. An initial slope of 0.05–0.1 m height and 1–2 m length (2.9–5.7°) was added in some runs.

After the sediments had been deposited, the amount of deposit in a fixed area was measured along the length of the flume. The sediments collected were dried and then weighed to determine the 'deposit density' (mass per unit bed area) profile along the flume. Details of the experimental procedure are presented elsewhere.

2.1. Results

Turbidity currents propagated with a typical flow velocity of 0.1–0.15 m/s in the proximal area, and travelled over 7 m. The surge-type currents had a 'head' approximately 0.1 m thick and a 'body' or 'tail' behind the head. The length of the head was no more than 1 m, though it was unable to be measured exactly in the proximal area. The tail of the flow was so diluted that a boundary with the ambient water was unclear. The current velocity in the tail diminished rapidly while some sediments still remained in suspension. No observation of a possible hydraulic jump or a reflected bore at slope breaks could be made, due to this vague boundary and the rapid waning of the flow.

Examples of the deposit density profiles are shown in Fig. 1 where circles represent the results for turbidity currents carrying coarser sediments and triangles for currents carrying finer sediments. There is generally a peak in the deposit density on the upstream flanks of the ridge, indicating preferential deposition caused by topographic effects. The preferential deposition occurred under various conditions with different ridge heights (0.036 m in panels a and b and 0.012 m in panel c), ridge lengths (1 m in panels a and c and 2 m in panel b) and incoming flow conditions controlled by the initial slope (0.1 in panels a and b and 0 in panel c).

The peaks in the deposit density profiles tend to be more distinct for turbidity currents with fine sediments. This tendency implies that these topographic effects are emphasised in deep-sea turbidity currents, where the relative size of the sediment is much smaller than in the laboratory-scale currents.

3. Numerical simulations

3.1. Flow equations

This study employs a layer-averaged, three-equation model in which equations for conservation of fluid mass, sediment mass and fluid momentum are solved simultaneously. This type of model has been widely used in the simulation of turbidity currents (e.g., Chu et al., 1979; Parker et al., 1986; Zeng and Lowe, 1997), and has the advantage of being less expensive computationally than a fully two-dimensional model. The layer-averaged, three-equation flow model is of the following form (Chu et al., 1979; Parker et al., 1986; Zeng and Lowe, 1997):

conservation of fluid mass

$$\frac{\partial h}{\partial t}+\frac{\partial}{\partial x}(uh)=E_{\mathrm{w}}u \tag{1}$$

conservation of momentum

$$\frac{\partial}{\partial t}(uh)+\frac{\partial}{\partial x}(u^2h)=-\frac{(\rho_{\mathrm{s}}-\rho_{\mathrm{w}})g}{2\rho_{\mathrm{w}}}\frac{\partial}{\partial x}(Ch^2)+$$

$$\frac{(\rho_{\mathrm{s}}-\rho_{\mathrm{w}})ghCS}{\rho_{\mathrm{w}}}-C_{\mathrm{d}}(1+\alpha)u^2 \tag{2}$$

conservation of sediment mass

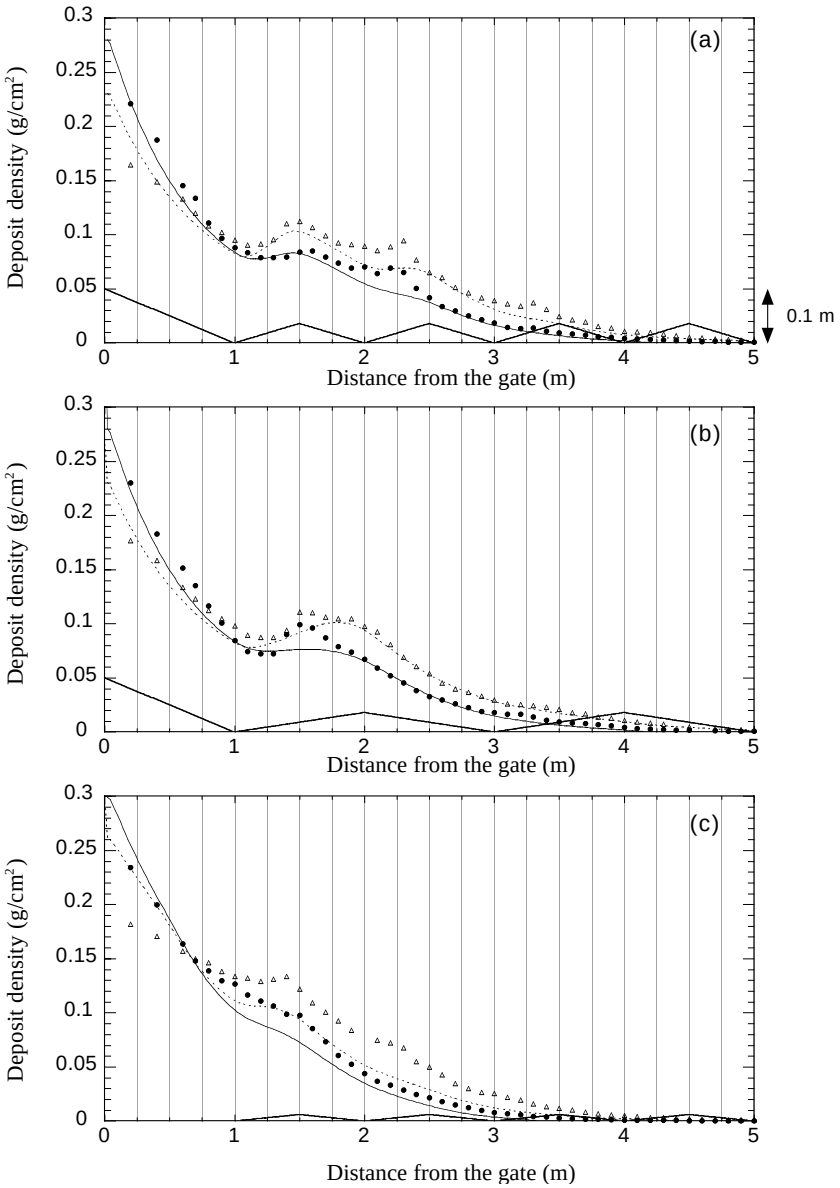

Fig. 1. The deposit density profiles of the laboratory experiments and the model predictions with the topography. (a) Initial slope of 0.1 (5.7°) for the first 1 m and four ridges of 0.036 m height and 1 m length. (b) Initial slope of 0.1 (5.7°) for the first 1 m and two ridges of 0.036 m height and 2 m length. (c) A horizontal bottom for the first 1 m and four ridges of 0.012 m height and 1 m length. The experimental results are plotted as circles for turbidity currents with coarse sediments, and as triangles for currents with fine sediments. The coarser sediments are represented by a mixture of 20% of the fine sand ($w_s = 1.0$ cm/s, $\phi = 3.0$), 50% of very fine sand ($w_s = 0.5$ cm/s, $\phi = 3.5$) and 30% of coarse silt ($w_s = 0.3$ cm/s, $\phi = 4.0$). The finer sediments are represented by a mixture of 40% of the fraction representing very fine sand ($w_s = 0.5$ cm/s), 50% of coarse silt ($w_s = 0.3$ cm/s) and 10% of medium silt ($w_s = 0.1$ cm/s, $\phi = 5.0$). The model predictions for turbidity currents with each sediment size are plotted as solid and broken lines respectively.

$$\frac{\partial}{\partial t}(Ch)+\frac{\partial}{\partial x}(uCh)=-F_d+F_e \quad (3)$$

where u is the flow velocity, h is the flow thickness, g is the acceleration due to gravity, E_w is the water entrainment coefficient, ρ_s and ρ_w are the densities of the sediment and ambient water, respectively, C is the volume concentration of the sediments, S is the bottom slope gradient, C_d is the drag coefficient, which has a value of 0.0035–0.005 (Komar, 1971, 1985), α is the ratio of the drag force at the upper flow surface to that at the bed, and F_d and F_e are the flux of sediment deposition and erosion, respectively. In Eq. 2, a constant value of 0.43 is used for α (e.g. Komar, 1969), though the value varies with the Froude number (Middleton, 1966b). The water entrainment coefficient, E_w, is determined from the empirical relationship (Fukushima et al., 1985):

$$E_w=\frac{0.00153}{0.0204+Ri}$$

where the Richardson number, Ri, is defined as

$$Ri=\frac{(\rho_s-\rho_w)ghC}{\rho_w U^2}$$

Introducing the non-dimensional quantities $X=x/x_0$, $U=u/u_0$ and $T=t/t_0$ yields for Eqs. 1–3:

$$\frac{\partial H}{\partial T}+\frac{\partial}{\partial X}(UH)=E_w U \quad (4)$$

$$\frac{\partial}{\partial T}(UH)+\frac{\partial}{\partial X}(U^2H)=$$

$$-\frac{R}{2}\frac{\partial}{\partial X}(CH^2)+RHCS-C_d(1+\alpha)U^2 \quad (5)$$

$$\frac{\partial}{\partial T}(CH)+\frac{\partial}{\partial X}(UCH)=\frac{-F_d+F_e}{u_0} \quad (6)$$

where $H=h/x_0$, $R=(\rho_s-\rho_w)/\rho_w$, $u_0=(gx_0)^{1/2}$, $t_0=(x_0/g)^{1/2}$, and x_0 is the length of the cells in the numerical calculations.

3.2. Erosion and deposition of sediments

The sediment flux at the bed is determined from the rates of deposition (F_d) and erosion (F_e). The rate of deposition, F_d, is described as the product of the settling velocity of sediment, w_s, and the fractional concentration of suspension at the bed, C_b. For multiple grain sizes, the sum of this product for each size population is used as the net rate of deposition. The sediment concentration at the bed, C_b, can be related to the layer-averaged concentration, C, by a factor of 2 (Garcia, 1993; Altinaker et al., 1996).

In order to describe the sediment entrainment from the bed, Fukushima et al. (1985) used a dimensionless number, Z, determined as

$$Z=\left(\frac{\sqrt{RgD_sD_s}}{\nu}\right)^{1/2}\frac{u_*}{w_s} \quad (7)$$

where D_s is the diameter of the sediment, $u_*=C_d^{1/2}u$ is the shear velocity, and ν is the kinematic viscosity of water. The rate of sediment entrainment, F_e, is described as w_sE_s with:

$$E_s=\begin{cases}0 & Z<5\\ 3\times10^{-12}Z^{10}\left(1-\frac{5}{Z}\right) & 5<Z<13.2\\ 0.3 & 13.2<Z\end{cases} \quad (8)$$

Though often used for turbidity current modelling (Fukushima et al., 1985; Parker et al., 1986; Zeng and Lowe, 1997), Eq. 8 is based on an empirical expression for sand-sized sediments. It should be noted that the bed surface on submarine levees is generally covered with fine-grained silts and muds that are easily consolidated. In order to describe the erosion of the deep-sea floor by turbidity currents, Mulder et al. (1998) assumed that erosion occurs if the shear stress created at the bottom of the flow, τ_b, exceeds the shear resistance of the sea bottom sediment, τ_s, using the quadratic stress law

$$\tau_b=C_d\rho_f u^2$$

and the relationship in which τ_s depends on the depth z:

$$\tau_s = az + b$$

Assuming that the maximum depth value for erosion, $z = (C_d\rho_f u^2 - b)/a$, occurs over 1 day, the rate of erosion (m/s) is determined as

$$F_e = (C_d\rho_f u^2 - b)/(a86400) \quad (9)$$

This erosion equation is sensitive to the values of a and b which must therefore be carefully calibrated by measurements. In this study, it is assumed that $a = 3.5$ and $b = 0.2$ based on the measurements of the shear strength of the marine sediment of the Saguenay Fjord (Mulder et al., 1998).

This study uses Eq. 8 for modelling of turbidity currents in laboratory experiments, in which sand-sized sediment was used, and Eq. 9 for simulating deep-sea turbidity currents.

3.3. Computation

The flow system is represented by space-fixed cells at which flow properties are evaluated. The temporal evolution of the field properties of the flow is computed from Eqs. 4–6 with the aid of Eq. 8 or Eq. 9. The computation employs staggered cells, in which the flow velocity (U) is calculated at the boundary of each cell while the flow depth (H) and the sediment concentration (C) are calculated at the centre of the cell. The advantages of this method are ease of discretisation and conservation of mass in every cell.

For a given $U_{k+1/2,t}$, the flow velocity at cell k is updated using the first-order accurate Euler-forward method as:

$$U_{k+1/2,t+1} = U_{k+1/2,t} + \Delta T\left(\frac{\partial U}{\partial T}\right)_{k+1/2,t} \quad (10)$$

where ΔT is the time increment and $\partial U/\partial T$ is determined from Eq. 5 as

$$\left(\frac{\partial U}{\partial T}\right)_{k+1/2,t} = -U_{k+1/2,t}\left(\frac{\partial U}{\partial X}\right)_{k+1/2,t} - \frac{R}{2}\left(\frac{\partial CH}{\partial X}\right)_{k+1/2,t} - \frac{RC}{2}\left(\frac{\partial H}{\partial X}\right)_{k+1/2,t} + R(CS)_{k+1/2,t} - \left(\frac{C_d(1+\alpha)U|U| + E_w U^2}{H}\right)_{k+1/2,t} \quad (11)$$

In the first term on the right-hand side of this equation, the gradient of the flow velocity is calculated using a first-order upwind difference scheme. The upwind difference scheme is employed to avoid numerical oscillation caused by the central difference scheme.

From Eqs. 4 and 6, the flow depth and the sediment concentration are updated as:

$$H_{k,t+1} = H_{k,t} + \Delta T\left(-\frac{\partial}{\partial X}(UH) + E_w U\right)_{k,t}$$

$$C_{k,t+1} = \frac{1}{H_{k,t+1}}\left(C_{k,t}H_{k,t} + \Delta T\left(-\frac{\partial}{\partial X}(UCH) + \frac{-F_d + F_e}{u_0}\right)_{k,t}\right)$$

The amount of deposited/eroded sediment is calculated from the sediment flux at the bed, and converted to bed thickness by assuming sediment porosity to be 0.5. Effects of post-depositional compaction are ignored.

The time step is constrained by the Courant–Friedrichs–Levy condition, i.e., is set not to exceed the grid interval divided by the flow velocity. The calculations are continued until the maximum sediment concentration is below 1% of the initial value.

3.4. Comparison with laboratory experiments

The numerical model is applied to the results of the laboratory experiments to check the validity of the model predictions. The initial and boundary conditions required in the calculations are given so as to be consistent with the corresponding laboratory experiments. The flow field in the 8-m-long flume is represented by 400 cells at 2-cm intervals. The settling velocity and the diameter of the sediments are represented by a mixture of three components: 20% of the fraction representing fine sand ($w_s = 1.0$ cm/s, $\phi = 3.0$), 50% of very

fine sand ($w_s = 0.5$ cm/s, $\phi = 3.5$) and 30% of coarse silt ($w_s = 0.3$ cm/s, $\phi = 4.0$). The finer sediments are represented by a mixture of 40% of the fraction representing very fine sand ($w_s = 0.5$ cm/s), 50% of coarse silt ($w_s = 0.3$ cm/s) and 10% of medium silt ($w_s = 0.1$ cm/s, $\phi = 5.0$).

The model predictions in Fig. 1 show good agreements with the experimental results for the positions of the peaks in the deposit density profiles. The peaks are, however, lower than those in the laboratory experiments. The higher peaks shown by the experimental results are likely to be attributed to effects ignored in the numerical model, e.g., erosion or reduced deposition at slope breaks due to increased shear stress associated with a hydraulic jump.

3.5. Application to natural settings

The model is applied to conditions that closely simulate spillover turbidity currents on submarine channel levees. The 20-km-long flow field is represented by 200 cells at 100-m intervals. A model turbidity current is generated by supplying stationary suspension at the upstream end of the flow field. The stationary suspension is represented by giving the constant height ($H_{k=1}$) and sediment concentration ($C_{k=1}$) of suspension for a given supply duration at the upstream-end cell, one side of which is bounded by no flux condition ($U_{k=1/2} = 0$). The flow velocity at the other side ($U_{k=3/2}$), and then all the parameters at the next cell, are computed from Eqs. 6 and 7.

The initial concentration is set at 0.1 or 0.5%, sufficiently less than the values used in calculations of the main head/body of the turbidity current in a channel (cf. 5–10% by Komar, 1969; 3–12% by Van Andel and Komar, 1969; 6% by Hiscott, 1994, 1–25% by Zeng and Lowe, 1997). This low concentration is selected in order to model spillover currents on backslopes of submarine channel levees where TC sediment-wave fields most commonly occur in nature. The low-concentration turbidity currents are also appropriate to sediment-wave formation by spreading (unconfined) flows (e.g. Wynn et al., 2000a,b). The initial height of the suspension is set at 20 or 50 m so as to be (i) of the same order as, but less than, the typical value of relief of submarine channels, and (ii) comparable to the difference of relief of the levees on opposite sides of the channel (Komar, 1969; Normark et al., 1980). The supply duration is set at 20 or 60 min, comparable to the passage time of a surge-type flow estimated from the deposition rate (20–52 min by Allen, 1991). The sediments are represented by a single grain size whose settling velocity is 0.002 or 0.5 cm/s.

In simulating sediment-wave formation, the deposition from turbidity currents is repeated for multiple flow events. The volume of deposits is converted to bed thickness by assuming the sediment porosity to be 0.5. As the bed thickness is small (< 0.15 m) compared to the scale of the topography, the thickness of a single turbidite bed is amplified 10 times and then added to the bed topography. This amplification assumes that the change of topography by a single turbidite bed is so little that the same thickness variations can be used for the next 10 turbidite beds. Post-depositional compaction and pelagic sedimentation can be ignored because they affect thickness in an almost uniform way and have little impact on the development of the wavy structures, even though the total thickness of the deposits is increased.

The model predicts the development of wavy structures by repeated deposition of turbidites onto an initially flat bed (Fig. 2). The initial conditions employed are 0.5% for sediment concentration, 50 m for suspension height, 20 min for suspension supply and 0.2 cm/s for settling velocity of sediments. Each layer represents 50 time intervals of calculation, corresponding to 500 turbidite beds in Fig. 2a. The wavy form occurs above the 3000th bed, in which the average slope gradient is 0.009 (0.5°). Wave formation is initiated by preferential deposition resulting from variation in bottom slope. Fig. 3 shows a clear correlation between the deposit thickness and the bottom slope gradient. In Fig. 3a, a first increase in deposit thickness occurs at the end of the steep slope near the source, and then results in variation in the bottom slope. The undulating bottom in turn leads to preferential deposition, as shown by the inverse correlation seen in Fig. 3, to form the wavy structure in Fig. 2. The waves, gradually

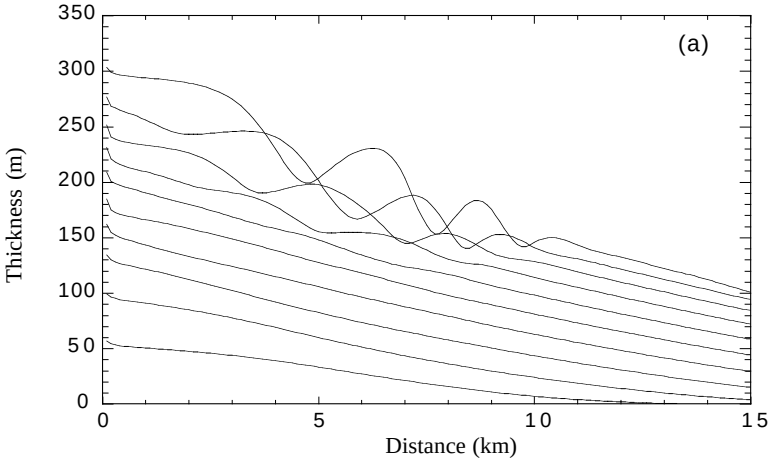
(a)
Thickness (m)
350
300
250
200
150
100
50
0
0
5
10
15
Distance (km)

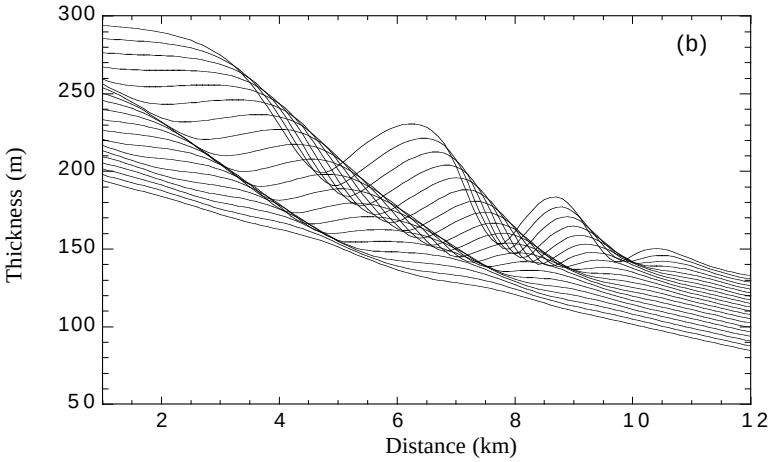
(b)
Thickness (m)
300
250
200
150
100
50
2
4
6
8
10
12
Distance (km)

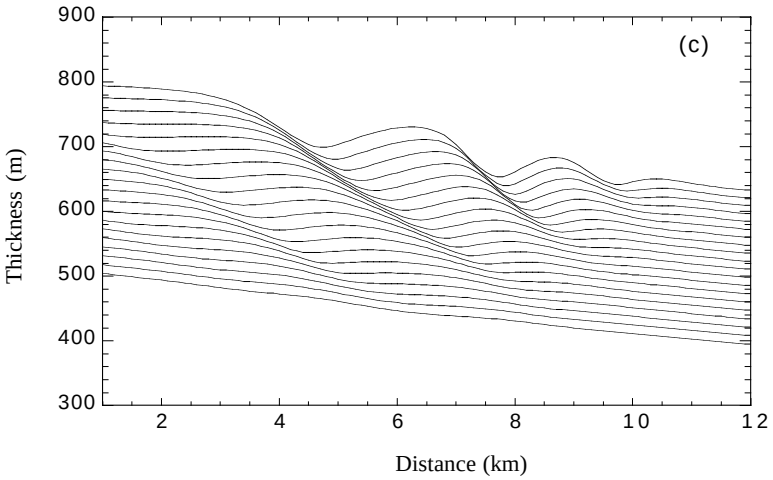
(c)
Thickness (m)
900
800
700
600
500
400
300
2
4
6
8
10
12
Distance (km)

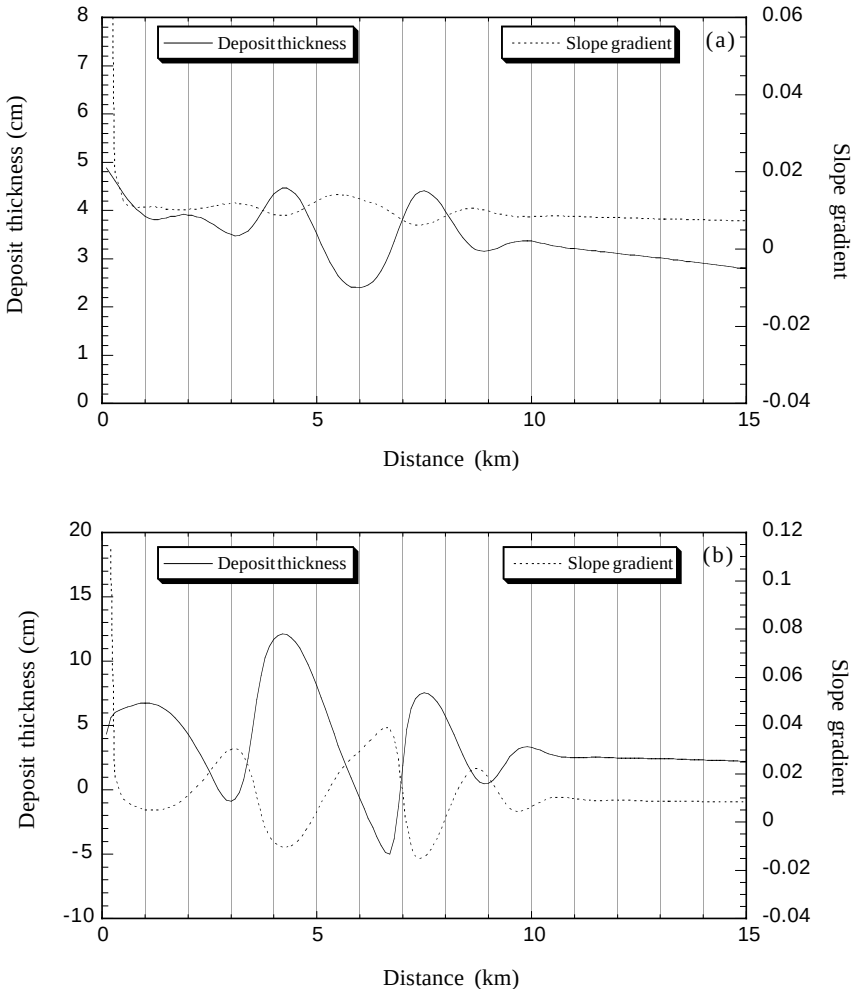

Fig. 3. The relationship between topography (dotted line) and thickness variation (solid line) of (a) 3000th and (b) 4000th turbidites in Fig. 2. Note the preferential deposition on the upstream flank of the wavy topography.

varying through time, finally have an apparent wavelength of 2–3 km and a wave height of 50 m in the 5000th bed. The enlarged Fig. 2b displays the upstream migration of the waveform, in which each layer represents 100 turbidites corresponding to the 3100th–5000th beds in Fig. 2a. The process of wave formation is discussed in detail later with another example.

The crossing of layers in Fig. 2a,b represents net erosion on the downstream flanks of the waves, where the slope gradient locally approaches 0.1 (5.7°). These erosional features are,

Fig. 2. The model prediction showing formation of wavy structures by repeated deposition of turbidites onto an initially flat bed. The initial conditions employed are 0.5% for sediment concentration, 50 m for suspension height, 20 min for suspension supply and 0.2 cm/s for settling velocity of sediments. (a) Each layer represents 50 time intervals of calculation, corresponding to 500 turbidite beds. The waves have an apparent wavelength of 1–3 km and a maximum wave height of 50 m. (b) Enlarged wavy structure between 3100th and 5000th turbidites in panel a. Each layer represents 100 turbidite beds. (c) Modified wavy structure by intercalating a uniform layer of 10 cm thickness in between each turbidite interval. This eliminates crossing of layers that would indicate net erosion.

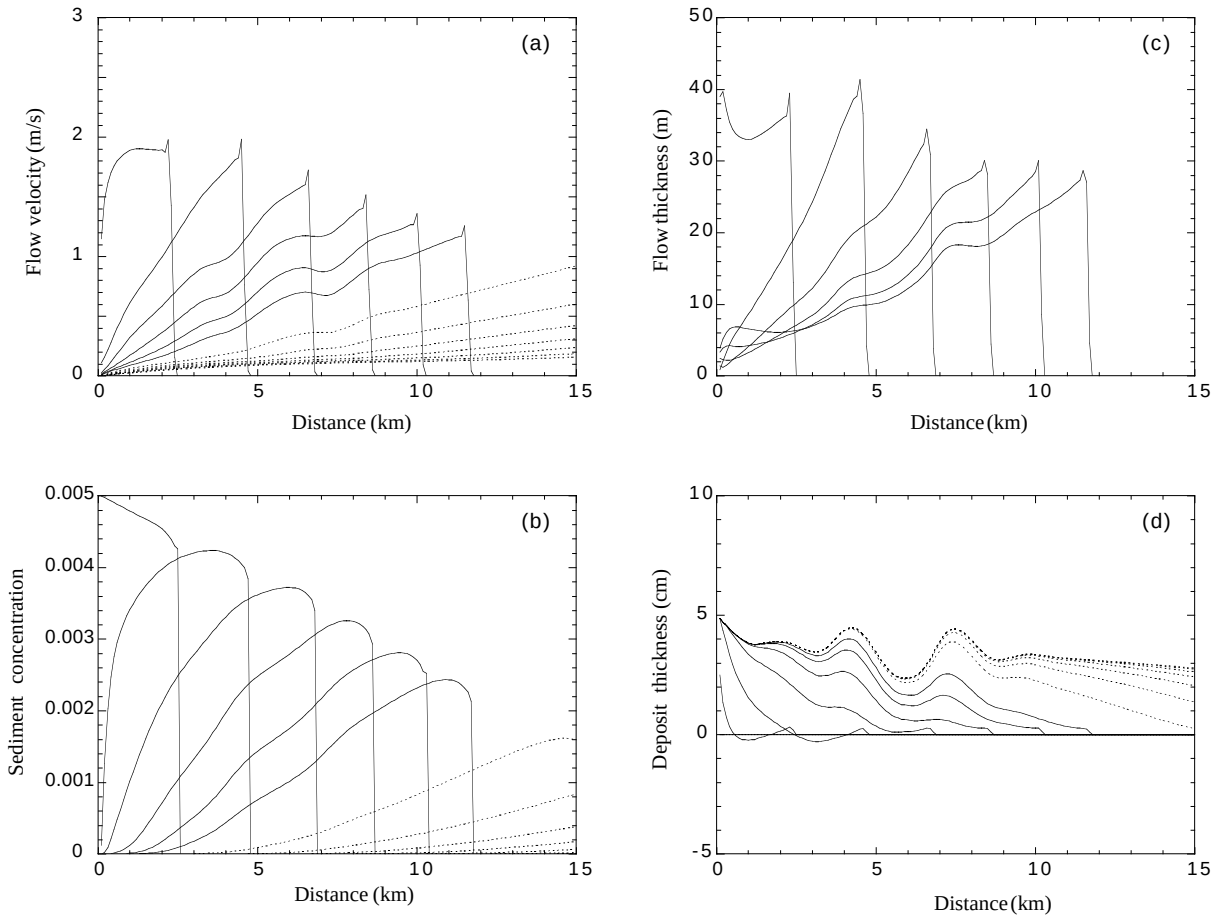

Fig. 4. Temporal evolution of (a) flow velocity, (b) sediment concentration, (c) flow thickness and (d) deposit thickness of the 3000th turbidity current in Fig. 2. Each line is at 20-min interval in the first 2 h (solid line) or 60 min (broken line).

however, possibly cancelled out by pelagic sedimentation intercalated with the turbidite beds. Fig. 2c shows an example where the crossing of layers is cancelled out by intercalating a uniform layer of 10 cm thickness in between each turbidite interval. In Fig. 2c, the total sediment thickness for wave formation is about 500–600 m.

Temporal evolution of flow conditions and deposit thickness are shown in Figs. 4 and 5, for turbidity currents in the initial (3000th) and developing (4000th) stage of wave formation, respectively. In each case, the turbidity current travels over 15 km within 3 h, with maximum flow velocity reaching 2 m/s. The sediment concentration decreases with time due to sediment loss by deposition and entrainment of ambient fluid. Due to the decrease in sediment concentration, the flows decelerate both with time and distance. The densitometric Froude number, $Fr_d = u/(RCgh)^{1/2}$, is varied with bottom slope and position in the flow. The calculated Froude number yields unrealistically large values in the rear part of the turbidity current due to the decrease in sediment concentration. The flows in the front part are subcritical ($Fr_d < 1$) on a horizontal bottom, and almost critical to supercritical ($Fr_d \approx 1$–1.2) in the initial stage of wave formation (3000th), while they are highly variable ($Fr_d \approx 0.6$–2.0) with the variation of bottom slope across wavy topography (4000th).

Topographic control on flow conditions is distinctly seen in the 4000th turbidity current (Fig.

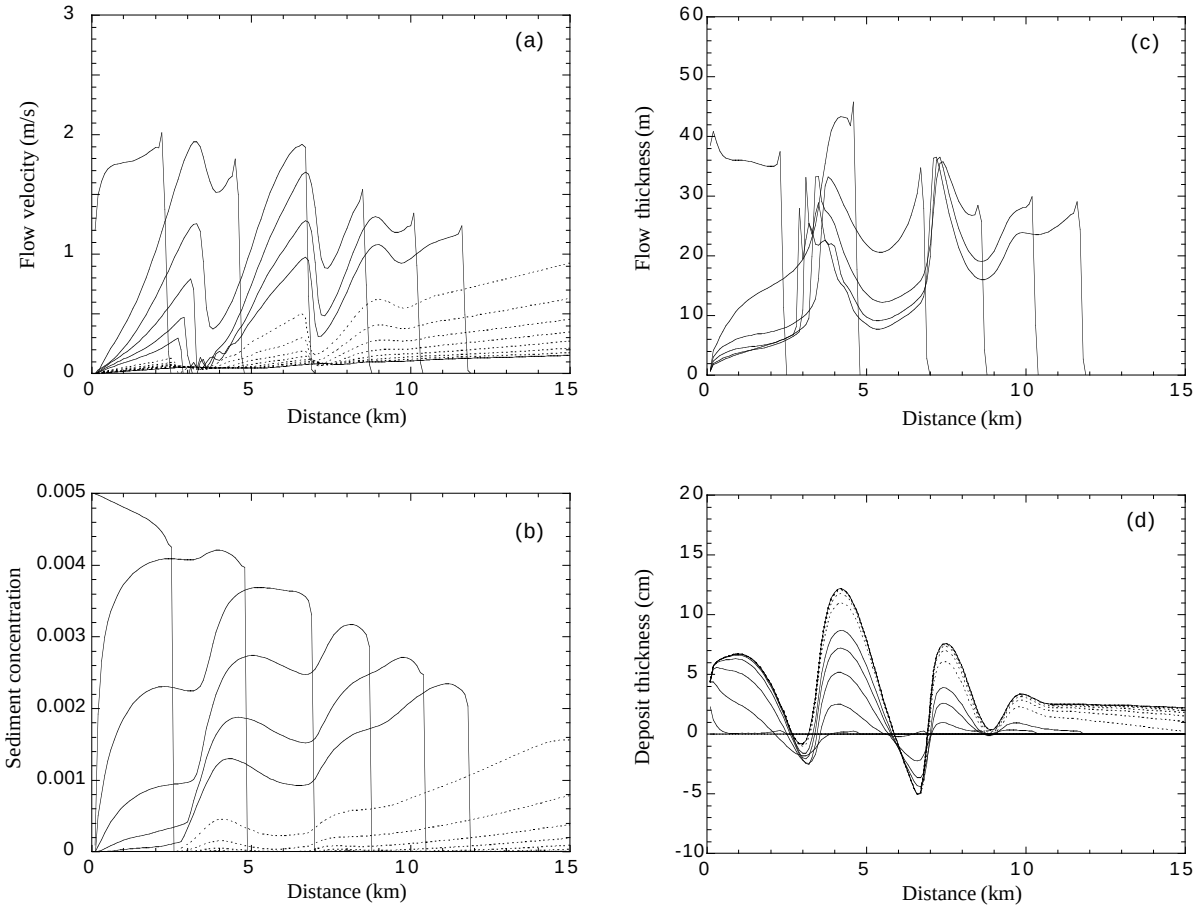

Fig. 5. Temporal evolution of (a) flow velocity, (b) sediment concentration, (c) flow thickness and (d) deposit thickness of the 4000th turbidity current in Fig. 2. Each line is at 20-min interval in the first 2 h (solid line) or 60 min (broken line). Note the preferential deposition on the upstream flank of the wavy topography. The decrease in the flow velocity and the increase in sediment concentration and flow thickness occur on the upstream flanks of the waves, indicating that flow is blocked at the crests.

5). The decrease in flow velocity and the increase in sediment concentration and flow thickness occurring on the upstream sides of the waves indicate that the flow is blocked at the crests. The flow is out of phase with the bed surface; the flow is thicker on the upstream flanks and thickest near the trough. The ponded sediments are preferentially deposited on the upstream sides and result in differential deposition between both sides of the wavy topography (Fig. 3). The differential deposition is also caused by local erosion or reduced deposition on the downstream flanks.

Temporal variation in deposit thickness and flow velocity at fixed points, 5 and 10 km from the source, is shown in Fig. 6. The flow velocity rapidly increases on arrival of the flow to reach the maximum and then gradually decreases with time, being halved within 40–50 min at the 5-km point and within 70 min at the 10-km point, respectively. The flow is decelerating while depositing its sediment: it takes 110–130 min at the 5-km point and 170–190 min at the 10-km point, respectively, for the deposit thickness to reach 90% of its final value.

The process of wave formation can be seen better in another example in Fig. 7, where the initial conditions are 0.1% for sediment concentration, 50 m for suspension height, 60 min for suspension supply and 0.5 cm/s for settling velocity of sediments. The wavy structure has an apparent wave-

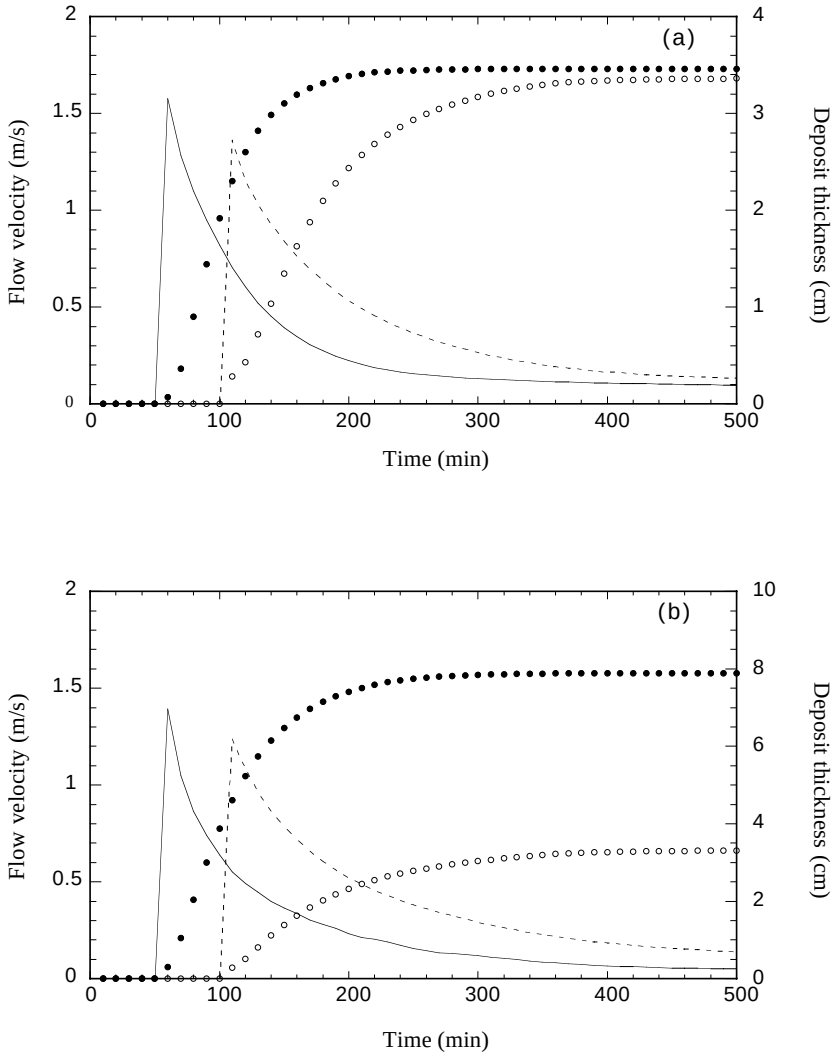

Fig. 6. Temporal variation of the deposit thickness and flow velocity of (a) 3000th and (b) 4000th turbidity currents in Fig. 2 at fixed points. Solid dots and lines show the deposit thickness and flow velocity at 5 km from the source, respectively. Open circles and dashed lines show those at 10 km from the source. The flow is decelerating while depositing its sediments.

length of 1–3 km and a maximum wave height of 70 m. It should be noted that each mound in the wavy structure develops individually, rather than as sinusoidal waves forming simultaneously. Each mound is produced by preferential deposition downstream from a change in bottom slope. The wave formation is initiated by the first slope break at 0.3–0.4 km from the source, which results from accumulation of concave-up profiles of turbidite beds on a flat bed (Fig. 7b). The first mound grows 0.6–0.7 km downstream from the slope break, and the process is repeated until the development of the third mound after deposition of 5000 turbidites.

4. Discussion

4.1. Laboratory experiments

The preferential deposition, if repeated, can result in upstream migration of the wave-like topog-

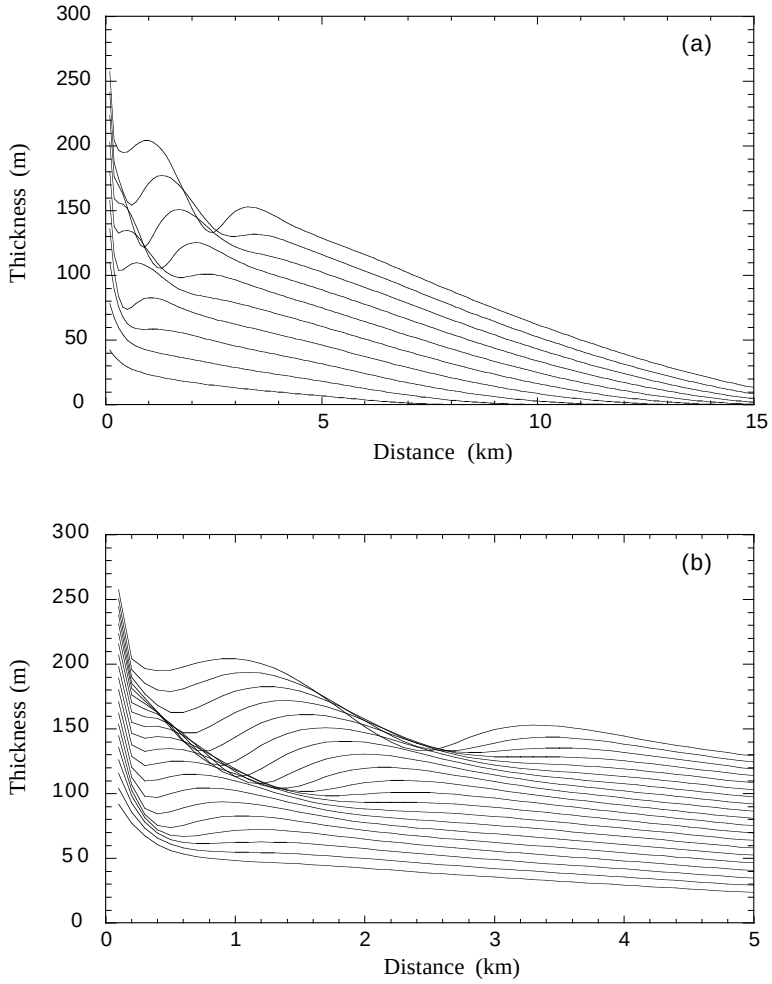

Fig. 7. The model prediction showing formation of wavy structures by repeated deposition of turbidites. The initial conditions employed are 0.1% for sediment concentration, 50 m for suspension height, 60 min for suspension supply and 0.5 cm/s for settling velocity of sediments. (a) Each layer represents 50 time intervals of calculation, corresponding to 500 turbidite beds. The waves have an apparent wavelength of 1–3 km and a maximum wave height of 70 m. (b) Enlarged wavy structure between 1200th and 5000th turbidites in panel a. Each layer represents 200 turbidite beds.

raphy as observed in deep-sea sediment waves. Possible causes of the preferential deposition in the experimental results are (i) deceleration of the flow on the upstream flank, (ii) blocking (ponding) effects of the topography and (iii) a hydraulic jump at the end of the downstream flank. At present, it is not possible to evaluate each effect independently due to lack of detailed measurements of the flow conditions and sedimentation process. However, it is clear that the preferential deposition is not necessarily related to antidune formation.

Antidunes typically form in flows with an overall Froude number around unity. According to the wave theory of bedforms, which considers steady flows over sinusoidal bed waves, antidunes are bedforms that are in-phase with the flow surface, and develop when the Froude number is between 0.844 and 1.77 (Allen, 1982a). Under the in-phase conditions the flow is expanded,

and therefore decelerated, on the upstream flank and contracted (decelerated) on the downstream flank. Upstream migration of antidunes occurs as a result of enhanced deposition on the upstream flank, matched by reduced deposition or erosion on the downstream flank.

In the experiments, however, such phase equivalence between the wave-like topography and the flow surface was not observed in a steady state. Even if the flow surface could be in-phase temporarily, i.e., the moving head could be slightly thicker at the crest and thinner at the trough, the length of the surge-type current was no more than the wavelength of the topography. This is inconsistent with the theory that considers a sinusoidal waveform at the surface of a steady flow. In addition, the preferential deposition occurred even when the incoming current was outside of the stability field of antidune formation ($Fr > 0.84$). The Froude number of the turbidity current starting on a horizontal bottom is about 0.7, as shown by a series of experiments in Middleton (1966a).

The experimental results indicate that preferential deposition on the upstream flank is a result of sea-floor topography. Therefore upstream migration of the waveform can occur in a turbidite sequence deposited over wavy topography, whatever the origin of the topography. If this is the case, the waveform in the turbidite sequence is likely to overlie the initial topography with little vertical variation in the wavelength. Such consistency can be commonly observed in fields of deep-sea sediment waves, which often preserve the irregular form of the underlying topography (e.g. Nakajima and Satoh, 2001). The origin of the wavy topography may be either natural undulations of the sea floor, slumps, large dunes or antidunes. For example, Nakajima and Satoh (2001) interpreted that the TC mudwaves on the levees of the Toyama deep-sea channel formed on top of large sand dunes, and their upstream migration resulted from differential draping of mud-capped silty turbidites (Fig. 8). Antidune development is also a possible origin for an underlying wavy topography on a relatively steep slope, though the relationship with upstream migration should be interpreted carefully.

4.2. Numerical simulations

The wavy structures in the model predictions show features similar to deep-sea sediment waves, regarding the dimensions and the pattern of internal layering. The numerical model, although oversimplified to evaluate the wave features quantitatively, presents qualitative speculations on the process of sediment wave formation by turbidity currents.

The wavy structure grows as a series of individual mounds that are gradually developed by preferential deposition after a change in bottom slope, rather than as sinusoidal waves forming simultaneously. As a mound grows, a new slope break on the downstream side of the mound then leads to generation of a second mound. Under the appropriate conditions, this process seems to occur almost simultaneously, and the structure appears to form as a sinusoidal wave (Fig. 2). It should be noted that any specific fluid motion, such as lee-waves and phase equivalence between the bed and fluid surface, is unnecessary for a cyclic, wavy structure to form. Therefore it is difficult to determine a critical or an appropriate condition for the wave formation, because the flow conditions are variable both in time and space.

The flow velocity decreases during sediment deposition both in time and space (Figs. 4a, 5a and 6). The waning flow observed at a fixed point is unlikely to form and maintain a single bedform, as indicated by the typical sequence of sedimentary structures in turbidites. The rapid deceleration suggests that formation of the wavy structure should not be interpreted as a bedform, e.g. an antidune, produced under steady and uniform flow conditions. Antidune development is also ruled out by a lack of phase equivalence between the flow and the bed surface. Therefore, the numerical model results indicate that antidune formation is an unlikely or unnecessary origin for the wavy structure, as shown by the results of laboratory experiments.

Antidune development is, on the other hand, still a possible origin for wave formation as a basement undulation underlying sediment waves. Supercritical turbidity currents are considered to be common in sediment-wave fields (e.g. Wynn et

al., 2000b), as they can occur on slopes in the order of 0.057° (Nakajima and Satoh, 2001). Antidune flow conditions are likely to be achieved only if the turbidity current is maintained steadily across the sea floor. Once an antidune is formed by an exceptionally steady flow, turbidite deposition is controlled by the undulations on the bed. The experimental results show that preferential deposition occurs on the upstream flank of the wave-like topography, resulting in upstream migration of the waves. A hydraulic jump, which commonly accompanies antidunes, can also take place and influence deposition under antidune conditions. It has been reported that maximum or preferential deposition occurs downstream from the jump both in open-channel flow (Jopling and Richardson, 1966) and in density currents (Hand, 1974; Garcia and Parker, 1989). The acute peaks in the deposit density variation in the experimental results (Fig. 1) are therefore possibly attributed to a hydraulic jump, which was too short-lived to observe visually. It is likely that antidune development and/or a hydraulic jump amplifies the preferential deposition, and is a trigger for the formation of sediment waves.

4.3. Limitation of the model

The numerical model, although predicting the formation of a wavy structure similar to TC sediment waves in the deep sea, includes some arbitrary assumptions for simplification, or due to lack of thorough understanding of turbidity current dynamics. The amplified bed thickness in the model computation exaggerates the variation in deposit distribution, causing rapid formation of the wavy structure. Therefore the number of turbidites and total sediment thickness required for the wave formation should be evaluated with care.

Another influential assumption in the model computation is that the same initial conditions are used for thousands of turbidity currents. A variety of size and flow conditions expected for turbidity currents in nature causes a possible delay of wave formation. Such variety in flow conditions, on the other hand, may play a positive role in the wave formation by causing non-uniformity in topography. For example, specific bedforms or localised deposition/erosion by one flow event would be a base upon which a wavy structure is developed. The influence of variation in flow conditions on the formation of TC sediment waves is complicated and still poorly understood.

The wavy structures in the model predictions are unlike natural TC sediment waves in that no more than 4–5 crests are developed during deposition of 5000 turbidite beds, whereas deep-sea analogues show more continuous waves. For example, the sediment waves in Fig. 8 with more than 10 crests are considered to consist of 6–7000 turbidites (Nakajima and Satoh, 2001; Nakajima, 1997). In some extensive sediment-wave fields, such as the La Palma sediment-wave field, simultaneous growth of waves over a long distance can be observed (Wynn et al., 2000a). Compared to these examples in nature, formation of the wavy structure in the model predictions is still slow, despite the exaggeration by the amplified bed thickness. Although some effects possibly accelerate the wave formation, the process shown by the numerical model is unlikely to develop an extensive, continuous sediment-wave field. This process should instead be applied to small wave fields, or combined with other processes when applied to extensive wave fields. A most likely combination is, as mentioned earlier, turbidite deposition on an initially undulated bottom, resulting in upstream migration by differential deposition, and downstream extension by formation of new mounds.

5. Conclusions

This study has presented new insights into the formation of sediment waves by turbidity currents. The results of the laboratory experiments indicate that preferential deposition on the upstream side of bed undulations can occur under a subcritical turbidity current. It implies that upstream migration of TC sediment waves is not necessarily related to antidunes but to topographic effects, such as (1) deceleration of the flow on the upstream flank of a ridge, (2) blocking effects of ridges and (3) a hydraulic jump at the

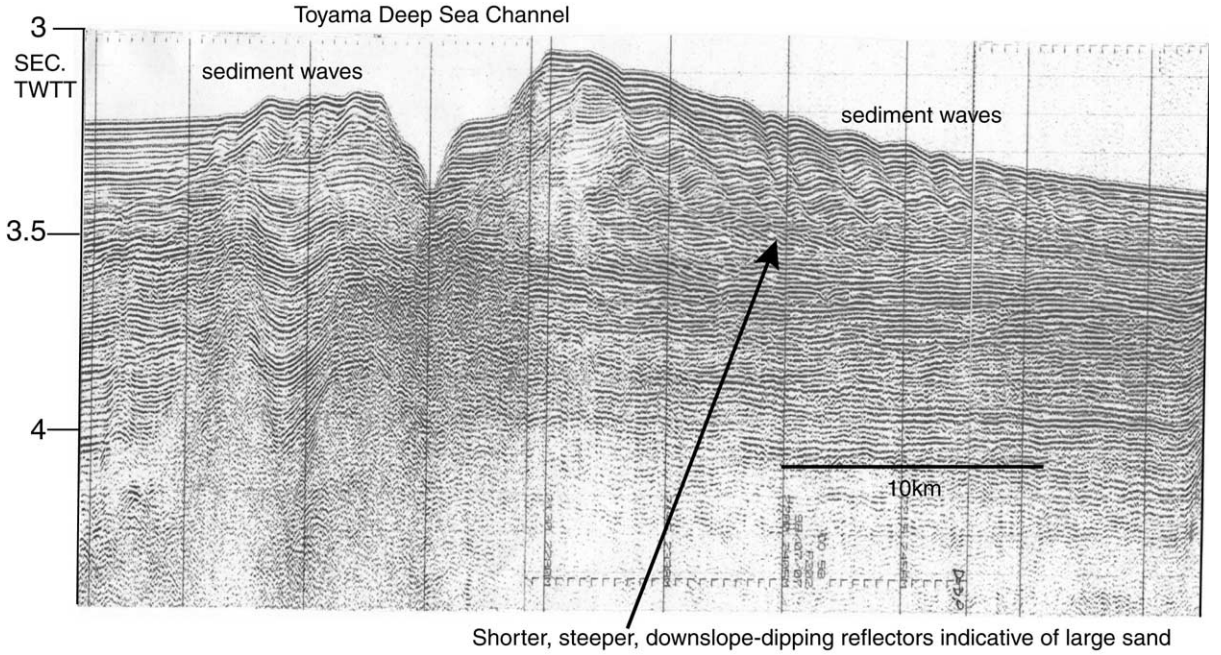

Fig. 8. An example of TC sediment wave on the levees of the Toyama deep-sea channel. The single-channel airgun reflection profile across the channel shows the internal layering of the sediment waves. The sediment waves are interpreted to form above large sand dunes, indicated by shorter, steeper, downslope dipping reflectors. Reproduced from Nakajima and Satoh (2001).

end of the downstream flank of a ridge. TC sediment waves should not be interpreted as antidunes based only on their upstream migration.

The results of the numerical simulation suggest a possible formation for a wavy structure in turbidite sequences. The wavy structure, very similar to deep-sea sediment waves, is interpreted as a series of mounds that are formed individually by topographic effects. The wave formation is initiated by preferential deposition behind a slope break and then followed by differential deposition on both sides of the mound. It is worth noting that wave formation in the model results requires no specific fluid motions, such as lee-waves or phase equivalence in a supercritical flow.

The wave formation as a series of mounds is, however, incompatible with extensive sediment-wave fields in nature. This process should only be applied to small wave fields, unless it is combined with other processes. The most likely combination is turbidite deposition on an initially undulating bottom, resulting in upstream migration and downstream extension of the undulation.

Acknowledgements

The authors would like to thank Fujio Masuda, Wonn Soh, Maarten Felix and Russell Wynn for their critical comments on an early version of the manuscript. Comments from Henry Pantin and an anonymous reviewer have helped the authors improve the manuscript. We also thank Tsuguo Sunamura and the members of the Geoenvironment Science Laboratory of Osaka University for their help in conducting the flume experiments, and Yukinobu Okamura and Mikio Satoh for collecting the seismic reflection profile shown in Fig. 8. This study was partly supported by funding from the Japan Society for the Promotion of Science for Young Scientists.

References

Allen, J.R.L., 1982a. Sedimentary Structures: their Character and Physical Basis, Vol. I. Elsevier, Amsterdam, 593 pp.
Allen, J.R.L., 1982b. Sedimentary Structures: their Character and Physical Basis, Vol. II. Elsevier, Amsterdam, 643 pp.

Allen, J.R.L., 1991. The Bouma division A and the possible duration of turbidity currents. J. Sediment. Petrol. 61, 291–295.

Altinaker, S., Graf, W.H., Hopfinger, E., 1996. Flow structure in turbidity currents. J. Hydraul. Res. 34, 713–718.

Bonnecaze, R.T., Huppert, H.E., Lister, J.R., 1993. Particle-driven gravity currents. J. Fluid Mech. 250, 339–369.

Bouma, A.H., 1962. Sedimentology of Some Flysch Deposits. Elsevier, Amsterdam, 168 pp.

Chu, F.H., Pilkey, W.D., Pilkey, O.H., 1979. An analytical study of turbidity current steady flow. Mar. Geol. 33, 205–220.

Flood, R.D., 1988. A lee wave model for deep-sea mudwave activity. Deep-Sea Res. 35, 973–983.

Fukushima, Y., Parker, G., Pantin, H.M., 1985. Prediction of ignitive turbidity currents in Scripps Submarine Canyon. Mar. Geol. 67, 55–81.

Garcia, M., 1993. Hydraulic jumps in sediment-driven bottom currents. J. Hydraul. Eng. 119, 1094–1117.

Garcia, M., Parker, G., 1989. Experiments on hydraulic jumps in turbidity currents near a canyon-fan transition. Science 245, 393–396.

Gladstone, C., Phillips, J.C., Sparks, R.S.J., 1998. Experiments on bidisperse, constant-volume gravity currents: propagation and sediment deposition. Sedimentology 45, 833–843.

Hand, B.M., 1974. Supercritical flow in density currents. J. Sediment. Petrol. 44, 637–648.

Hiscott, R.N., 1994. Loss of capacity, not competence, as the fundamental process governing deposition from turbidity currents. J. Sediment. Res. A64, 209–214.

Jopling, A.V., Richardson, E.V., 1966. Backset bedding developed in shooting flow in laboratory experiments. J. Sediment. Petrol. 36, 821–825.

Komar, P.D., 1969. The channelized flow of turbidity currents with application to Monterey deep-sea fan channel. J. Geophys. Res. 74, 4544–4558.

Komar, P.D., 1971. Hydraulic jumps in turbidity currents. Geol. Soc. Am. Bull. 82, 1477–1488.

Komar, P.D., 1985. The hydraulic interpretation of turbidites from their grain sizes and sedimentary structures. Sedimentology 32, 395–407.

Middleton, G.V., 1966a. Experiments on density and turbidity currents I. Motion of fluid. Can. J. Earth Sci. 3, 523–546.

Middleton, G.V., 1966b. Experiments on density and turbidity currents II. Uniform flow of density currents. Can. J. Earth Sci. 3, 627–637.

Middleton, G.V., Neal, W.J., 1989. Experiments on the thickness of beds deposited by turbidity currents. J. Sediment. Petrol. 59, 297–307.

Miles, J.W., 1968. Lee waves in a stratified flow. Part 1. Thin barrier. J. Fluid Mech. 32, 549–567.

Mulder, T., Syvitski, J.P.M., Skene, K.I., 1998. Modeling of erosion and deposition by turbidity currents generated at river mouths. J. Sediment. Res. 68, 124–137.

Nakajima, T., 1997. Turbidite Sedimentation along the Toyama Deep Sea Channel in the Japan Sea. Doctoral thesis, Kyoto University, 108 pp., unpubl.

Nakajima, T., Satoh, M., 2001. The formation of large mudwaves by turbidity currents on the levees of the Toyama deep-sea channel, Japan Sea. Sedimentology 48, 435–463.

Normark, W.R., Hess, G.R., Stow, D.A.V., Bowen, A.J., 1980. Sediment waves on the Monterey Fan levee: a preliminary physical interpretation. Mar. Geol. 37, 1–18.

Parker, G., Fukushima, Y., Pantin, H.M., 1986. Self-accelerating turbidity currents. J. Fluid Mech. 171, 145–181.

Piper, D.J.W., Savoye, B., 1993. Processes of late Quaternary turbidity current flow and deposition on the Var deep-sea fan, north-west Mediterranean Sea. Sedimentology 40, 557–582.

Queney, P., 1948. The problem of air flow over mountains: a summary of theoretical studies. Bull. Am. Meteorol. Soc. 29, 16–26.

Van Andel, T.H., Komar, P.D., 1969. Ponded sediments of the Mid-Atlantic Ridge between 22° and 22° north latitude. Geol. Soc. Am. Bull. 80, 1163–1190.

Wynn, R.B., Masson, D.G., Stow, D.A.V., Weaver, P.P.E., 2000a. Turbidity current sediment waves on the submarine slopes of the western Canary Islands. Mar. Geol. 163, 185–198.

Wynn, R.B., Weaver, P.P.E., Ercilla, G., Stow, D.A.V., Masson, D.G., 2000b. Sedimentary processes in the Selvage sediment-wave field, NE Atlantic: new insights into the formation of sediment waves by turbidity currents. Sedimentology 47, 1181–1197.

Yih, C., 1969. Stratified flows. Annu. Rev. Fluid Mech. 1, 73–110.

Zeng, J., Lowe, D.R., 1997. Numerical simulation of turbidity current flow and sedimentation. I. Theory. Sedimentology 44, 67–84.